J Arid Land (2025) 17(5): 644–663
doi: 10.1007/s40333-025-0100-0; CSTR: 32276.14.JAL.02501000

Science Press Springer-Verlag

Mechanical properties of surface soil in alpine meadow and its relationship with soil cracking in Qinghai Province, China

ZHANG Hailong[1], ZHU Haili[1,2*], WU Yuechen[1], XU Pengkai[1], HONG Chenze[1], LIU Yabin[1,2], LI Guorong[1,2], HU Xiasong[1,2]

[1] School of Geological Engineering, Qinghai University, Xining 810016, China;
[2] Key Laboratory of the Cenozoic Resources and Environment on the North Rim of the Qinghai-Xizang Plateau, Xining 810016, China

Abstract: Surface soil cracking in alpine meadows signifies the transition of degradation from quantitative accumulation to qualitative deterioration. Quantitative research remains insufficient regarding changes in the mechanical properties of degraded meadow soils and the mechanical thresholds for cracking initiation. This study explored the relationships between surface cracking and the physical properties, tensile strength, and matrix suction of root-soil composites in alpine meadow sites with different stages of degradation (undegraded (UD), lightly degraded (LD), moderately degraded (MD), and heavily degraded (HD)) under different water gradients (high water content (HWC), medium water content (MWC), and low water content (LWC)) corresponding to different drying durations at a constant temperature of 40.0°C. The Huangcheng Mongolian Township in Menyuan Hui Autonomous County, Qinghai Province, China was chosen as the study area. The results indicated that as the degradation degree of alpine meadow intensified, both water content of root-soil composite and the fine grain content of soil decreased. In contrast, the root-soil mass ratio and root area ratio initially increased and then decreased with progressive degradation. Under a consistent water content, the tensile strength of root-soil composite followed a pattern of MD>HD>LD>UD. The peak displacement of tensile strength also decreased as the degradation degree of alpine meadow increased. Both the tensile strength and matrix suction of root-soil composite increased as root-soil water content decreased. A root-soil water content of 30.00%–40.00% was found to be the critical threshold for soil cracking in alpine meadows. Within this range, the matrix suction of root-soil composite ranged from 50.00 to 100.00 kPa, resulting in the formation of linear cracks in the surface soil. As the root-soil water content continued to decrease, liner cracks evolved into branch-like and polygonal patterns. The findings of this study provide essential data for improving the mechanical understanding of grassland cracking and its development process.

Keywords: degradation; alpine meadow; root-soil composite; tensile strength; matrix suction; grassland crack

Citation: ZHANG Hailong, ZHU Haili, WU Yuechen, XU Pengkai, HONG Chenze, LIU Yabin, LI Guorong, HU Xiasong. 2025. Mechanical properties of surface soil in alpine meadow and its relationship with soil cracking in Qinghai Province, China. Journal of Arid Land, 17(5): 644–663. https://doi.org/10.1007/s40333-025-0100-0; https://cstr.cn/32276.14.JAL.02501000

*Corresponding author: ZHU Haili (E-mail: qdzhuhaili@163.com)
Received 2025-01-26; revised 2025-03-15; accepted 2025-05-05

1 Introduction

As a vital ecological barrier on the Qinghai-Xizang Plateau, alpine grasslands play a crucial role in maintaining the ecological security of the surrounding plateau areas, and their influence even extends to parts of Central Asia (Immerzeel et al., 2010). In recent decades, the grasslands experienced extensive degradation due to a combination of factors, including intensified extreme climate events on the Qinghai-Xizang Plateau, global warming, prolonged drying trends, and increasingly frequent human economic activities. These factors lead to a significant reduction in biodiversity and severe damage to the structures and functions of alpine grassland ecosystems (Victor and Hua, 2010; Miehe et al., 2019). Miehe et al. (2019) pointed out that grassland destruction and soil erosion often begin with the formation of polygonal cracks in the sod layer. The presence of surface cracks disrupts the water and heat balance, initiating a shift in the degradation process from gradual and quantitative changes to more abrupt and qualitative changes. In alpine meadows, soil surface cracking accelerates water evaporation and loss, alters the soil's water and thermal conditions (Fan et al., 2020), and results in changes to the soil structure. The cracks diminish the soil's mechanical properties (Lozada et al., 2015), compromise its permeability, and disrupt the movement of both moisture and solutes (Greve et al., 2010; Zhang et al., 2014). Additionally, surface cracks hinder the growth and development of plant roots (Xiong et al., 2008), thereby exacerbating grassland degradation and soil erosion, and ultimately leading the ecosystem into a vicious cycle. Therefore, it is essential to understand the mechanisms by which surface cracks affect the physical, chemical, and mechanical properties of root-soil composite.

Soil cracking is a typical form of tensile failure and is primarily governed by two key mechanical factors: matrix suction and the tensile strength of the soil itself (Tang et al., 2018). Tang et al. (2021) showed that a decrease in water content leads to the generation of matrix suction, further causing soil shrinkage. When the tensile stress field induced by matrix suction exceeds the tensile strength of the soil, cracks begin to form (Xu et al., 2018). Numerous studies have been conducted to explore the mechanical properties of matrix suction and tensile strength in root-soil composite. Peron et al. (2009a) measured the critical matrix suction (90.00–100.00 kPa), at which soil cracks begin to form, using a tensiometer. Ni et al. (2017) found that the difference in the water contents of root system and surrounding soil, referred to as the water absorption capacity of root, significantly impacts the magnitude and distribution of matrix suction. Liu et al. (2019) proposed that plant roots in vegetated soils effectively increase the air entry volume of soil, and found that the matrix suction in root-soil composite is 1.5–2.0 times higher than that in non-rooted soils. In addition, relevant scholars conducted in-depth research on the hydraulic characteristics of root-soil composite (Leung et al., 2015; Yildiz et al., 2019). They quantitatively revealed the relationship between root characteristics and soil hydraulic conductivity (Cui et al., 2024) as well as the permeability coefficient (Gholami et al., 2024). However, their model did not fully incorporate the mechanical interactions at root-soil interfaces (Lu et al., 2020; Gholami et al., 2024). When explaining the soil cracking mechanism, the above mentioned studies overlooked the mechanical role of roots.

In terms of the study of tensile strength of root-soil composite, Schwarz et al. (2010) investigated the tensile strengthening effect of plant roots on soil and found that the friction force at root-soil interface varies with the root diameter, thereby influencing the tensile strength of root-soil composite. Li et al. (2020) conducted *in situ* tensile tests to study the tensile characteristics of the root-soil composite of alpine meadows at different degrees of degradation in Henan County, Qinghai Province, China. They proposed that as the meadow deteriorates, the root quantity decreases and the root system composition changes, while the tensile strength of the root-soil composite tends to decrease with the aggravation of degradation. Zhou and Wang (2019) concluded that the root material has a high tensile strength, and it significantly enhances the tensile strength of soil and limits the development

of cracks. As soil water content decreases following crack initiation, matrix suction progressively increases (Xu et al., 2018). When matrix suction exceeds a critical threshold, the stress intensity factor at crack tips surpasses the soil's tensile strength, thereby inducing crack propagation and deepening (Zheng, 2003). Under wetting-drying and freeze-thaw cycles, crack formation and evolution in grasslands and farmlands are driven by water content fluctuations, which arise from coupled mechanical-hydraulic interactions.

Prior studies predominantly examine individual variables (e.g., root growth or root decay, soil gradation, and evaporation) in isolation, neglecting systematic quantification of their hydromechanical coupling effects (Cheng et al., 2024; Yuliana et al., 2025). Given that alpine meadow topsoil contains abundant fine roots with high water absorption and enhanced tensile and shear resistance (Fan et al., 2020; He et al., 2025), this study focused on two key mechanical drivers of cracking: matrix suction and tensile strength. By treating root-soil water content as a control variable, we developed a mechanistic linkage between surface cracking and the interplay of matrix suction and tensile strength. Through mechanical analysis, we identified a critical water content threshold for crack initiation. These findings offer scientific insights for conserving and rehabilitating alpine meadows in the eco-fragile Qinghai-Xizang Plateau.

2 Study area

The experimental site is located in Huangcheng Mongolian Township, Menyuan Hui Autonomous County, Haibei Tibetan Autonomous Prefecture, Qinghai Province, China (37°39′54″–37°40′3″N, 101°10′40″–101°10′44″E; 3200–3250 m a.s.l.) (Fig. 1). This region experiences a typical plateau continental climate. The annual average temperature fluctuates between 0.4°C and 2.5°C. The average temperature in the warmest month is 10.1°C and that in the coldest month is –15.0°C. The diurnal temperature variations are significant, with an average difference of 15.7°C over many years. The area is characterised by a cold climate, long winters, short summers, and distinct seasonal shifts between cold and warm periods. The average annual evaporation rate is 1192.000 mm, while the average annual precipitation is 524.100 mm, and the majority of the precipitation occurs in May and September, accounting for 83.41% of the total annual precipitation (Wu et al., 2024).

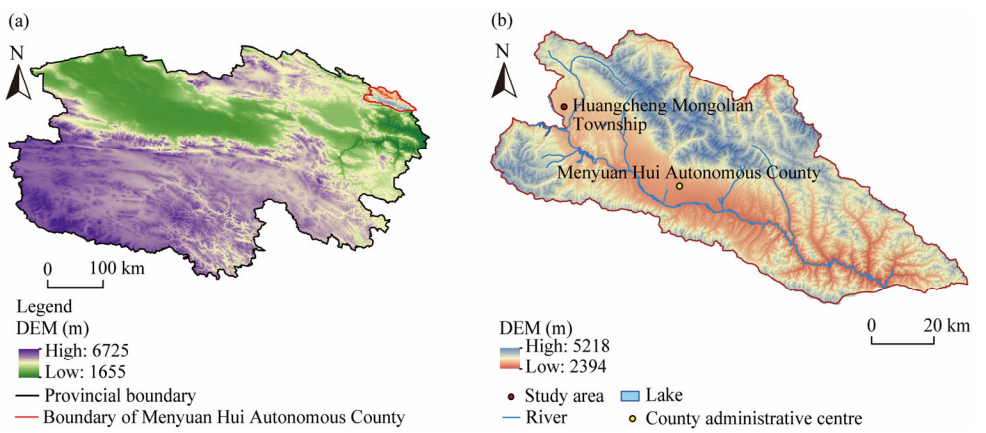

Fig. 1 Location of Menyuan Hui Autonomous County in Qinghai Province (a) and location of the study area in Huangcheng Mongolian Township, Menyuan Hui Autonomous County (b). DEM, digital elevation model.

To investigate the surface cracking characteristics of alpine meadows in different regions and degradation stages, we conducted extensive surveys across alpine meadows in Qilian County, Menyuan Hui Autonomous County, Henan Mongolian Autonomous County, and Dari

County in Qinghai Province. The results revealed that the surface layer of *Kobresia pygmaea* C. B. Clarke alpine meadows exhibited varying degrees of cracking in areas with different stages of degradation. The most prominent case occurred in Huangcheng Mongolian Township, Menyuan Hui Autonomous County, Qinghai. There, household-based free grazing practices led to divergent grassland degradation and succession patterns under different management approaches. This spatial variation enabled researchers to study meadow degradation stages using space-for-time substitution methods (Wang et al., 2016; Duan et al., 2020). Based on factors such as the herbaceous plant growth, surface vegetation coverage, and other conditions within the area and following the standard of Parameters for Degradation, Sandification, and Salification of Rangelands (General Administration of Quality Supervision, Inspection and Quarantine of the People's Republic of China, 2004), we classified the alpine meadow sites in the study area into four degrees of degradation: undegraded (UD), lightly degraded (LD), moderately degraded (MD), and heavily degraded (HD). This classification was conducted using the principle of spatial sequence rather than temporal succession (Wang et al., 2016; Duan et al., 2020). The survey revealed that as the meadow degradation intensified, the vegetation coverage decreased. The dominant plant species, including grasses such as *Poa crymophila* Keng, *Elymus nutans* Griseb., *Kobresia pygmaea* C. B. Clarke, and *Kobresia humilis* (C. A. Mey. ex Trautv.) Serg., were gradually replaced by forbs such as *Potentilla bifurca* L. and *Saussurea pulchra* Lipsch. The surface cracks in the alpine meadow evolved from simple linear cracks to more composite branch-like and polygonal cracks (Fig. 2). This was accompanied by an increase in the proportion of bare areas and terrain collapse (Table 1).

Fig. 2 Developmental morphological of surface cracks in alpine meadows. (a), linear fracture; (b), dendritic fracture; (c), polygonal fracture.

3 Materials and methods

3.1 Field sampling

In the study area, we selected four alpine meadow plots representing different degradation degrees (UD, LD, MD, and HD). Each plot comprised a 150.00 m×150.00 m square. The linear distances between the four plots ranged from 3 to 15 km. To ensure randomization and representativeness and to avoid road interference, all sampling plots were located away from the boundaries of the test plots about 50.00 m. We established three sampling points along the diagonal of each plot, spaced at 50.00 m intervals. In May 2024, we measured basic physical properties, root parameters, tensile strength, and matrix suction in the UD, LD, MD, and HD plots and collected *in situ* samples, with three replicates per test. Since surface cracks in the study area's alpine meadows primarily formed within the 0.00–10.00 cm soil layer, we set the sampling depth to 0.00–10.00 cm.

We collected *in situ* samples using a small ring cutter (inner diameter: 6.18 cm, height: 2.00 cm), aluminum boxes, and sealed plastic bags to determine water content, dry density, and particle size distribution in the laboratory (Fig. 3a). To ensure the plant roots accurately represented their effects on surface cracking and mechanical properties of alpine meadow,

Table 1 Basic characteristics of alpine meadow sites with different degrees of degradation in the study area

Degradation degree	Dominant species	Coverage of Gramineae and Cyperaceae (%)	Vegetation coverage (%)	Status of surface crack
Undegraded (UD)	*Kobresia humilis* (C. A. Mey. ex Trautv.) Serg., *Elymus nutans* Griseb., and *Poa crymophila* Keng	73.00–85.00	95.00–100.00	The meadow surface layer doesn't exhibit apparent crack.
Lightly degraded (LD)	*Kobresia pygmaea* C. B. Clarke, *Poa crymophila* Keng, and *Saussurea pulchra* Lipsch	62.00–72.00	80.00–95.00	Simple linear cracks can be observed.
Moderately degraded (MD)	*Kobresia pygmaea* C. B. Clarke, *Gentiana dahurica* Fischer, and *Saussurea pulchra* Lipsch	45.00–58.00	60.00–85.00	Branch-like cracks can be observed and the crack area doesn't exceed 5.00% of the total plot area.
Heavily degraded (HD)	*Potentilla bifurca* L., *Anaphalis lactea* Maxim. and *Carex capillifolia* (Decne.) S. R. Zhang	30.00–43.00	40.00–60.00	Irregular polygonal cracks can be observed, accompanied by bare ground and collapse areas around the cracks.

we extracted root-soil composite samples (diameter: 10.00 cm, depth: 0.00–10.00 cm) using a JC-802 profile root drill (Nanjing Soil Instrument Factory Co., Ltd., Nanjing, China) for laboratory root parameter analysis (Fig. 3b). For matrix suction measurements, we collected *in situ* samples with a large ring cutter (inner diameter: 10.00 cm, height: 6.37 cm), while uniaxial tensile samples were obtained using a custom mold (height: 10.00 cm) (Fig. 3c). The integrity of the underground root system of plants and their above-ground stems and leaves was maintained during the sampling process. The *in situ* root-soil composite samples were packed into wooden boxes, surrounded by sponges and transported to the laboratory. The field preparation of the *in situ* root-soil samples was completed in a timely manner (within 1–2 d) in order to minimise errors in the root-soil composite samples caused by environmental influences, thus effectively ensuring the reasonableness and correctness of test results.

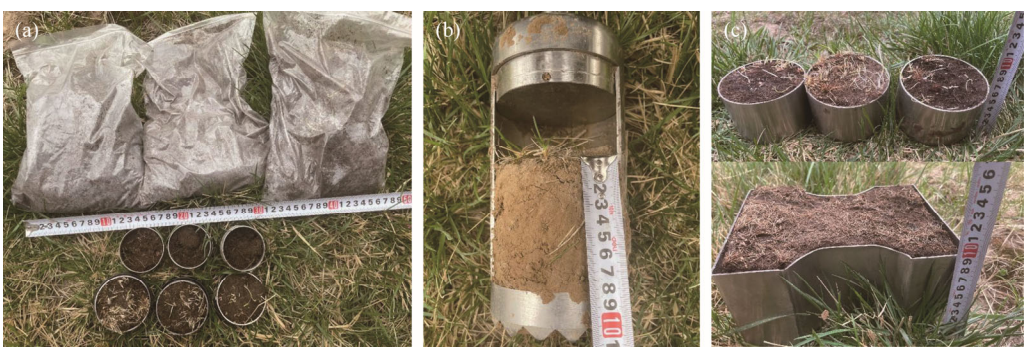

Fig. 3 Field sampling. (a), soil physical properties samples; (b), plant root parameters; (c), tensile and matrix suction samples.

3.2 Determination of physical characteristics of root soil system and plant root system parameters

According to the Geotechnical Test Method Standard (GB/T50123-2019) (Ministry of Housing and Urban-Rural Development of the People's Republic of China, 2019), we determined the root-soil water content (w_{sr}), soil water content (w_s), and root water content (w_r) of different degraded samples by drying method, the dry density (ρ_d) by the ring knife method, and the soil particle classification by screening analysis method. We calculated the uniformity coefficient (C_u) and curvature coefficient (C_c) to analyze the uniformity and

continuity of soil particles. Among them, the determination of w_s and w_r required first sieving the root and soil in the taken root soil sample and weighing the quality of fresh root and wet soil respectively to obtain the quality of fresh root and wet soil. Then, to obtain the mass of dry root and soil, we dried the fresh root and wet soil at 65.0℃ for 48 h. The root diameter of the root-soil composite samples was measure by vernier caliper. The specific calculation formulas for each parameter are as follows (Preti and Giadrossich, 2009):

$$w_{sr} = \frac{(m_{fr} + m_{ws}) - (m_s + m_r)}{m_s + m_r} \times 100\%, \tag{1}$$

$$w_r = \frac{m_{fr} - m_r}{m_r} \times 100\%, \tag{2}$$

$$w_s = \frac{m_{ws} - m_s}{m_s} \times 100\%, \tag{3}$$

$$\rho_d = \frac{\rho}{1 + 0.01 w_{sr}} = \frac{m_{fr} + m_{ws}}{V \times (1 + 0.01 w_{sr})}, \tag{4}$$

$$C_u = \frac{d_{60}}{d_{10}}, \tag{5}$$

$$C_c = \frac{{d_{30}}^2}{d_{60} \times d_{10}}, \tag{6}$$

$$R_s = \frac{m_r}{m_s} \times 100\%, \tag{7}$$

$$\mathrm{RAR} = \frac{A_r}{A} = \frac{\sum_{i=1}^{n} \frac{\pi {d_i}^2}{4}}{A} \times 100\%, \tag{8}$$

where w_{sr} is the root-soil water content (%); m_{fr} is the fresh root mass (g); m_{ws} is the wet soil mass (g); m_r is the dry root mass (g); m_s is the dry soil mass (g); w_r is the root water content (%); w_s is the soil water content (%); ρ_d is the dry density (g/cm^3); ρ is the wet density (g/cm^3); V is the volume of ring knife, and it is 60 cm^3 in this study; C_u is the uniformity coefficient; d_{60} is the particle size at which the mass of soil smaller than this size on the particle size distribution curve accounts for 60.00% of the total mass of soil (mm); d_{10} is the particle size at which the mass of soil smaller than this size on the particle size distribution curve accounts for 10.00% of the total mass of soil (mm); C_c is the curvature coefficient; d_{30} is the particle size at which the mass of soil smaller than this size on the particle size distribution curve accounts for 30.00% of the total mass of soil (mm); R_s is the root-soil mass ratio (%); RAR is the root area ratio (%); n is the total number of roots; A_r is the total cross-sectional area of the root system in the root-soil composite sample profile (mm^2); A is the area of the root-soil composite sample profile (mm^2); and d_i is the diameter of the i^{th} root (mm).

3.3 Water content setting

Because the root-soil composite structure and water-holding capacity varied with degradation degrees in the study area, the initial root-soil water content differed across samples. Directly assigning fixed root-soil water content values under different gradient conditions for controlled testing would have been inappropriate. Therefore, we adopted the root-soil water content gradient method used in saturated expansive soil drying experiments (Tang et al., 2012; Gu et al., 2023). Based on the characteristic evaporation rate curve, which consists of constant rate stage, deceleration rate stage, and residual stage, we set root-soil water content gradients corresponding to these three stages (Tang et al., 2012).

Therefore, we carried out a preliminary test for evaporation rate curve determination. Firstly, root-soil composite samples were subjected to simulated rainfall using a 2 L adjustable

air-pressure spray can with a wetting intensity of 55.3 mm/h. Water was applied until the weight of the root-soil composite sample stabilized. The watered samples were then placed in a constant temperature and humidity drying oven (ATS-WS-408T; Shanghai ETISON Instrument Technology Co., Ltd., Shanghai, China) at 40.0℃ for drying, and the surface crack development images were observed and taken over time every 12 h during the drying process. Finally, the test is completed when the root-soil water content is 0.00%. According to the water content curve, we defined the initial values of root-soil water content corresponding to the three stages as three gradients: high water content (HWC), medium water content (MWC), and low water content (LWC). The corresponding drying time for HWC, MWC, and LWC were 0, 48, and 84 h, respectively (Fig. 4).

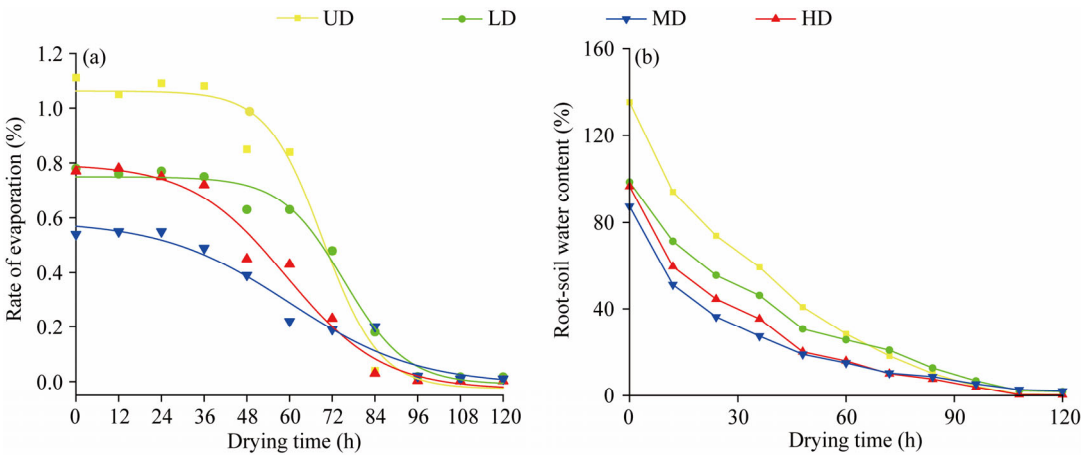

Fig. 4 Evaporation rate curve (a) and water content curve (b) of root-soil composite sample determined by this study. UD, undegraded; LD, lightly degraded; MD, moderately degraded; HD, highly degraded.

3.4 Tensile test

The microcomputer horizontal tensile testing machine (TFL-3KN, Shanghai Tuofeng Instrument Technology Co., Ltd., Shanghai, China) consists of a displacement sensor (range: 0.000–600.000 mm, accuracy: 0.001 mm), a tension sensor (range: 0.00–0.20 kN, accuracy: 0.01 N), a sample loading fixture, a tensile mould, and a data acquisition system (Fig. 5). To avoid stress concentration in the tensile mould, the research team designed a dumbbell-shaped mould based on the existing indoor uniaxial tensile testing device (Huang et al., 2018). The length of the connection between the tensile mould was increased to 7.00 cm. We mounted root-soil composite tensile samples onto the platform of the tensile testing apparatus, setting the elongation rate to 1 mm/min. The data acquisition system recorded tensile stress and displacement at 0.1 s. The test terminated when the measured tension dropped sharply and stabilized. Simultaneously, the system automatically generated stress-displacement curves spanning the entire loading process. To ensure data reliability, we conducted three experimental replicates. The tensile strength of root-soil composite was calculated as follows:

$$P = \frac{F}{S}, \tag{9}$$

where P is the tensile stress of the root-soil composite (kPa); F is the peak froce in the root-soil composite (N); and S is the area of the tensile fracture cross-section (mm^2).

3.5 Matrix suction test

This experiment employed a soil water potential monitoring system to measure the matrix suction of four root-soil composite samples. The system primarily consisted of a ZL6 data

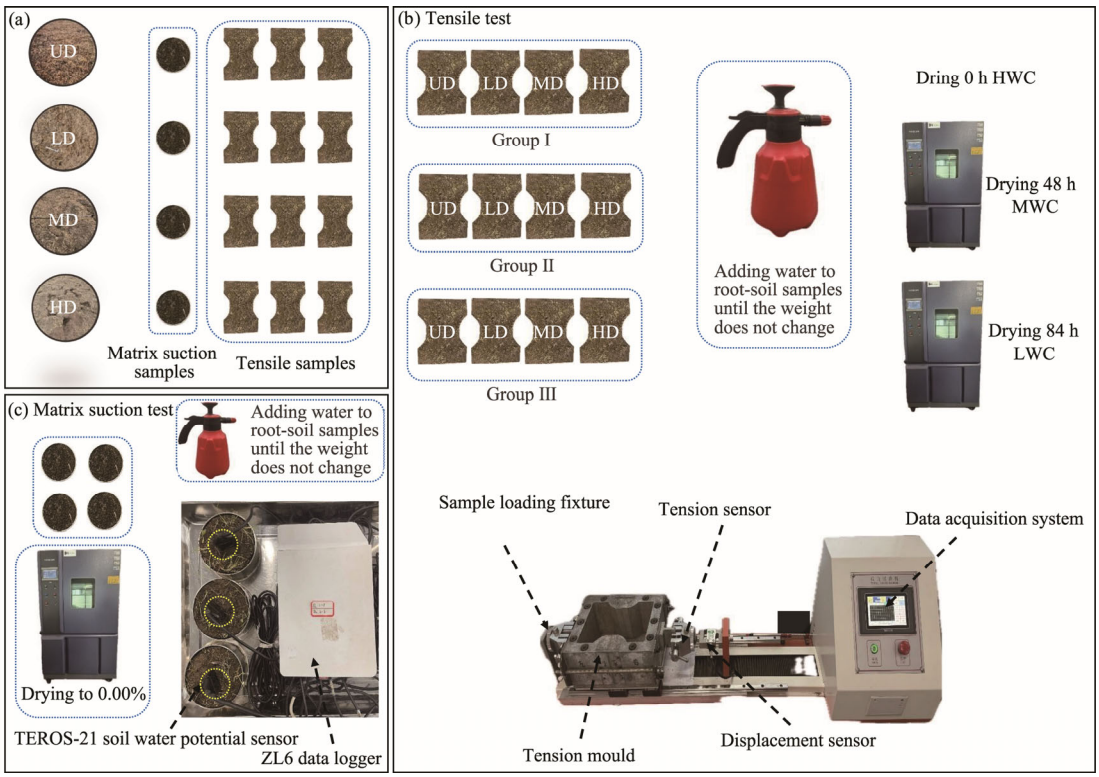

Fig. 5 Schematic diagram of test process. (a), field sampling; (b), drying experiment and tensile test; (c), matrix suction test. HWC, high water content; MWC, medium water content; LWC, low water content.

logger (METER USA Ltd., Washington City, USA) and TEROS-21 soil water potential sensors (METER USA Ltd., Washington City, USA). Firstly, we saturated the large ring knife samples of root-soil composite to constant weight. Then, we wrapped each TEROS-21 sensor probe with a thin layer of moist soil to ensure full contact with the surrounding soil, installed them at 2.00 cm below the sample surface, and placed the assemblies in a 40.0℃ constant-temperature drying oven. The test is concluded when the root-soil water content is 0.00%. The stabilized value tested by ZL6 data logger was the final matrix suction of the root-soil composite (Fig. 5). Throughout the process, we measured the evaporated water mass and matrix suction at 12 h intervals, calculating the matrix suction change rate to analyze its temporal variation across degradation degrees. The specific calculation formula follows:

$$v_{\varphi} = \frac{\varphi_{t+1} - \varphi_t}{h}, \tag{10}$$

where v_{φ} is the rate of change in matrix suction (kPa/h); φ_t and φ_{t+1} are the matrix suction measured at the t^{th} and $(t+1)^{\text{th}}$ times (kPa); and h is the time interval between each matrix suction measurement (h; in this research, h is 12 h).

3.6 Statistical analysis

All of the experimental data and calculation results were first input into an Excel file (Microsoft, Redmond, USA) and then imported into Origin 2022 software (OriginLab Corporation, Northampton, USA) for further analysis. All of the relevant charts and curves in this study were plotted in Origin 2022 to ensure clear visualization and accurate presentation of the results. We utilized the MATLAB R2023b software (MathWorks Corporation, Natick, Massachusetts, USA) to analyze the relationship among root-soil water content, matrix suction, and tensile strength of root-soil composites with different degrees of degradation.

4 Results

4.1 Physical properties of root-soil composite

As shown in Table 2, as the degree of degradation of the alpine meadow intensified, significant changes occurred in the physical properties of root-soil composite from the 0.00–10.00 cm soil layer. The dry density of root-soil composite increased from 0.39 g/cm^3 in the UD plot to 0.66 g/cm^3 in the HD plot, i.e., a 69.20% increase, indicating that with increasing degradation, the porosity of soil decreases, the soil particles become more tightly packed, and the compactness of the soil increases. The root-soil water content and the water contents of root and soil exhibited decreasing trends. Specifically, the root-soil water content decreased from 93.40% in the UD plot to 38.56% in the HD plot. In addition, compared with the UD plot, the water contents of root system and soil in the HD plot decreased from 140.42% and 56.39% to 31.34% and 33.34%, respectively. As the alpine meadow degraded from UD to HD, the root-soil mass ratio and root area ratio in the 0.00–10.00 cm soil layer initially increased and then decreased. The root-soil mass ratio and root area ratio reached their maximum values (22.29% and 32.31%, respectively) in the MD stage and then decreased by 42.56% and 46.22%, respectively, in the HD stage. This pattern is attributed to the degradation process in the study area, in which the aboveground vegetation becomes stunted and the number of roots in the shallow soil increases sharply. The root growth in both the horizontal and vertical directions intertwine, forming a dense and thick layer of felt. In conclusion, the root-soil mass ratio and root area ratio in the shallow soil peaked in the MD stage. However, as cracks developed and the surface area became more bare and subsided, the root content of soil began to decrease.

Table 2 Basic characteristics of root-soil composite in alpine meadows with different degrees of degradation

Degradation degree	ρ_d (g/cm^3)	w_{sr} (%)	w_r (%)	w_s (%)	R_s (%)	RAR (%)
UD	0.39±0.03	93.40±7.21	140.42±13.55	56.39±5.70	13.58±2.12	14.75±2.05
LD	0.57±0.02	76.25±5.37	113.30±14.14	47.82±6.52	16.45±1.48	18.11±1.42
MD	0.60±0.01	48.86±10.47	82.63±11.27	35.50±3.90	22.29±5.52	32.31±18.48
HD	0.66±0.02	38.56±12.73	31.34±1.44	33.34±3.93	12.80±1.56	17.37±12.49

Note: ρ_d, dry density; w_{sr}, root-soil water content; w_r, root water content; w_s, soil water content; R_s, root-soil mass ratio; RAR, root area ratio. Mean±standard deviation.

The intensified degradation of alpine meadows also affects the composition and gradation characteristics of soil particles. As shown in Table 3, the content of fine grain (<0.075 mm) decreased from 23.70% in the UD plot to 10.25% in the HD plot, showing a reduction of 56.75%. Meanwhile, the content of coarse particles (>0.250 mm) increased from 34.05% in the UD plot to 61.35% in the HD plot, with a growth of 80.15%. This indicated that during the degradation process, the particle size distribution of soil becomes coarser. Additionally, both the uniformity coefficient and curvature coefficient of soil particles initially decreased and then increased. The uniformity coefficient of the UD plot was 8.78, indicating that the soil was well-graded sandy silt. However, with increasing degradation degree, the uniformity coefficient decreased to 7.45 in the HD plot, demonstrating a decrease in the uniformity of soil particles with increasing degradation. The curvature coefficient gradually decreased from 1.93 to 0.78 with increasing degradation, indicating that the particle gradation worsened.

4.2 Tensile strength characteristics of root-soil composite

Figure 6 shows the tensile stress-displacement curves of the root-soil composites in the four different degradation plots (UD, LD, MD, and HD) under three water content gradients (HWC, MWC, and LWC). The peak stress in the diagram represents the tensile strength of root-soil composite. The results indicated that with increasing alpine meadow degradation, the tensile

strength of root-soil composite initially increased and then decreased, following the order UD<LD<HD<MD. The tensile strength values of the root-soil composite samples from the MD plot under the LWC, MWC, and HWC gradients were the highest, reaching 50.49, 45.58, and 36.11 kPa, respectively. These values were 70.92%, 148.53%, and 134.74% higher than those of the root-soil composite samples from the UD plot, respectively. Under all three water content gradients, the peak displacements at the tensile stresses for the root-soil composites were 22.000–25.000 (LWC), 26.000–30.000 (MWC), and 30.000–36.000 mm (HWC). As root-soil water content increased, the tensile displacement of root-soil composite gradually increased, indicating a higher ductility. When the root-soil water content increased, the amount of free water at root-soil interface also increased, enhancing the lubrication, reducing the friction, and making the root system more likely to slip and pull out rather than break in the soil, which weakened the tensile reinforcement effect of root system on soil.

Table 3 Basic characteristics of sand particle at the upper soil layer in alpine meadows with different degrees of degradation

Degradation degree	Granule composition (%)			C_u	C_c	Gradation type	Soil type
	>0.250 mm	0.075–0.250 mm	<0.075mm				
UD	34.05±12.56	41.25±10.36	23.70±6.56	8.78	1.93	Well-graded	SS
LD	36.60±14.11	53.21±12.29	13.93±8.42	3.69	1.17	Poorly-graded	CS
MD	53.04±20.53	39.03±18.46	7.93±6.53	4.44	0.96	Poorly-graded	CS
HD	61.35±22.95	29.95±17.34	10.25±4.34	7.45	0.78	Poorly-graded	CS

Note: C_u, uniformity coefficient; C_c, curvature coefficient; SS, silt sand; CS, clay sand. Well-graded means the particles with various diameters are well-distributed in the soil; Poorly-graded means the particles with various diameters are uneven distributed in the soil. Mean±standard deviation.

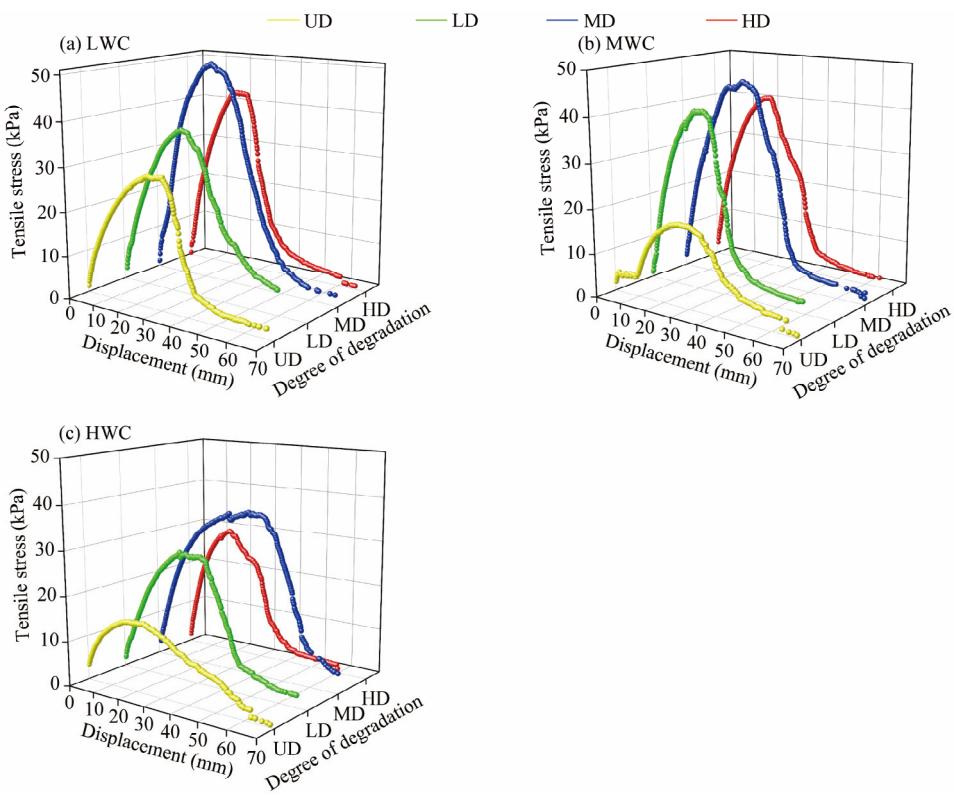

Fig. 6 Tensile stress-displacement curve of root-soil composite under different water content gradients. (a), LWC; (b), MWC; (c), HWC.

Based on the stress-deformation characteristics of root-soil composite with varying degradation degrees, the study divided the tensile failure process of root-soil composite under tensile force into four consecutive stages: Stage I—elastic deformation, Stage II—elastic-plastic deformation, Stage III—root fracturing and local soil failure, and Stage IV—overall failure (Fig. 7). At the Stage I, the tensile stress and displacement of root-soil composite exhibited a proportional relationship, and the root-soil composite could return to its initial state after the removal of tensile stress. At this stage, the tensile displacement of the root-soil composite from the UD plot was 7.200 mm and the tensile stress was 19.80 kPa, while the root-soil composite from the HD plot had a lower tensile displacement of 4.500 mm and a higher tensile stress of 22.10 kPa, indicating that intensified degradation leads to enhanced tensile strength, which is related to changes in the root-soil mass ratio across different degrees of degradation. As tensile stress increased, the root-soil composite entered the elastic-plastic deformation stage, exhibiting irreversible plastic deformation. At this stage, the tensile stress no longer increased significantly with displacement, and the increase was relatively small comparing with the Stage I. When the root-soil composite was subjected to partial tensile stress, microcracks began to form and gradually expanded. This occurred earliest in the root-soil composite from the HD plot, followed by the MD, LD, and UD successively. As the tensile stress increased further, the root-soil composite entered Stage III, in which the tensile stress of the root-soil composites from UD, LD, MD, and HD plots all reached their peaks. The root-soil composite from the MD plot exhibited the tensile strength (i.e., the highest tensile stress) of 50.49 kPa, which was significantly higher than those of the root-soil composites from the UD, LD, and HD plots, indicating that the synergistic effects of root-soil mass ratio and root-area ratio in the MD plot effectively enhanced the tensile strength of root-soil composite. The root-soil composite from the UD plot exhibited the greatest peak tensile displacement of 30.000–36.000 mm, while the root-soil composite from the HD plot exhibited the lowest displacement of 17.000–22.000 mm, suggesting that intensified degradation reduces the ductility of root-soil composite. During this stage, localized failure phenomena occurred in the root-soil composites and the crack propagation intensified. At this stage, the tensile stress-displacement curve exhibited two distinct characteristics. First, the curve exhibited noticeable sawtooth-like nonlinear fluctuations. This phenomenon occurred because roots with different diameters and strengths fractured at different stress degrees during the tensile process. Each time a group of roots fractured, it caused a downward fluctuation in the tensile stress-displacement curve. As the remaining unfractured roots continued to bear the tensile load, the tensile stress gradually increased until the next group of roots fractured. Second, there was a noticeable reduction in the tensile stress, which caused the curve to drop sharply. This was due to the insufficient interfacial bond strength between the roots and soil particles in the root-soil composites from the UD and LD plots. As a result, roots slipped within soil, leading to fluctuations in the curves. With increasing degradation, from UD to MD, the root-soil mass ratio of soil increased, and the ductility of root-soil composite increased, indicating better tensile properties under tensile stress. The overall failure stage was observed, in which a large number of root fractures and damage to the soil structure occurred. At this stage, the overall strength of root-soil composite decreased to a critical degree, and the tensile stress decreased to approximately 0.00–10.00 kPa, resulting in fracturing and overall instability of root-soil composite. These stages collectively revealed the composite mechanical behaviour and the failure mechanisms of root-soil composite under tensile stress.

4.3 Matrix suction characteristics of root-soil composite

The matrix suction of root-soil composite exhibited an increasing trend with decreasing root-soil water content across all degradation levels of alpine meadows (Fig. 8). Meanwhile, the increase in matrix suction varied significantly among root-soil composite with different degradation degrees. In the root-soil composite from the UD plot, due to the high vegetation

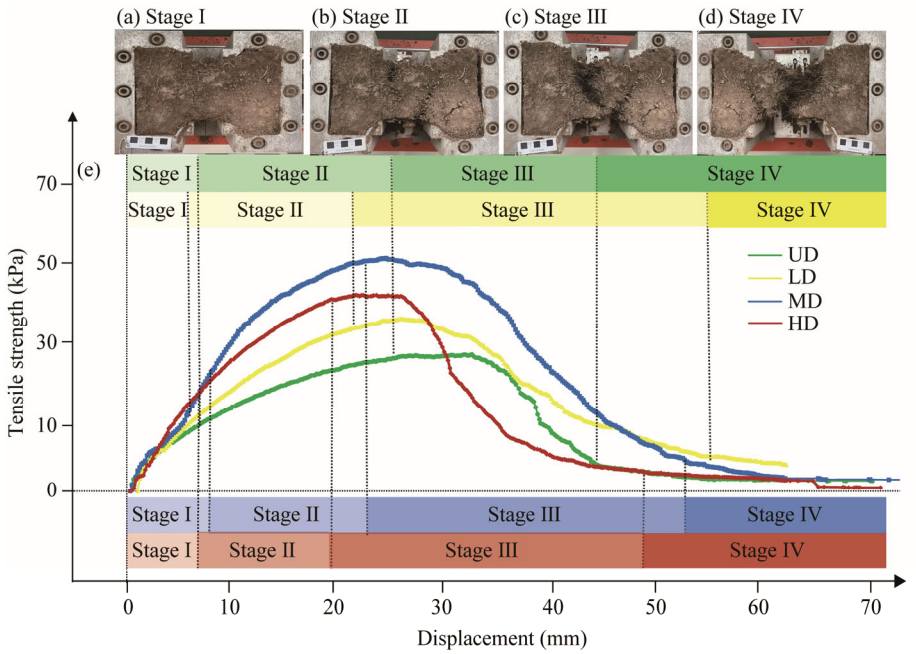

Fig. 7 Stage classification diagram of tensile stress-displacement curve under LWC condition. (a), elastic deformation stage (Stage I); (b), elastic-plastic deformation stage (Stage II); (c), root fracturing and local soil failure stage (Stage III); (d), overall failure stage (Stage IV); (e), tensile stress-displacement curve.

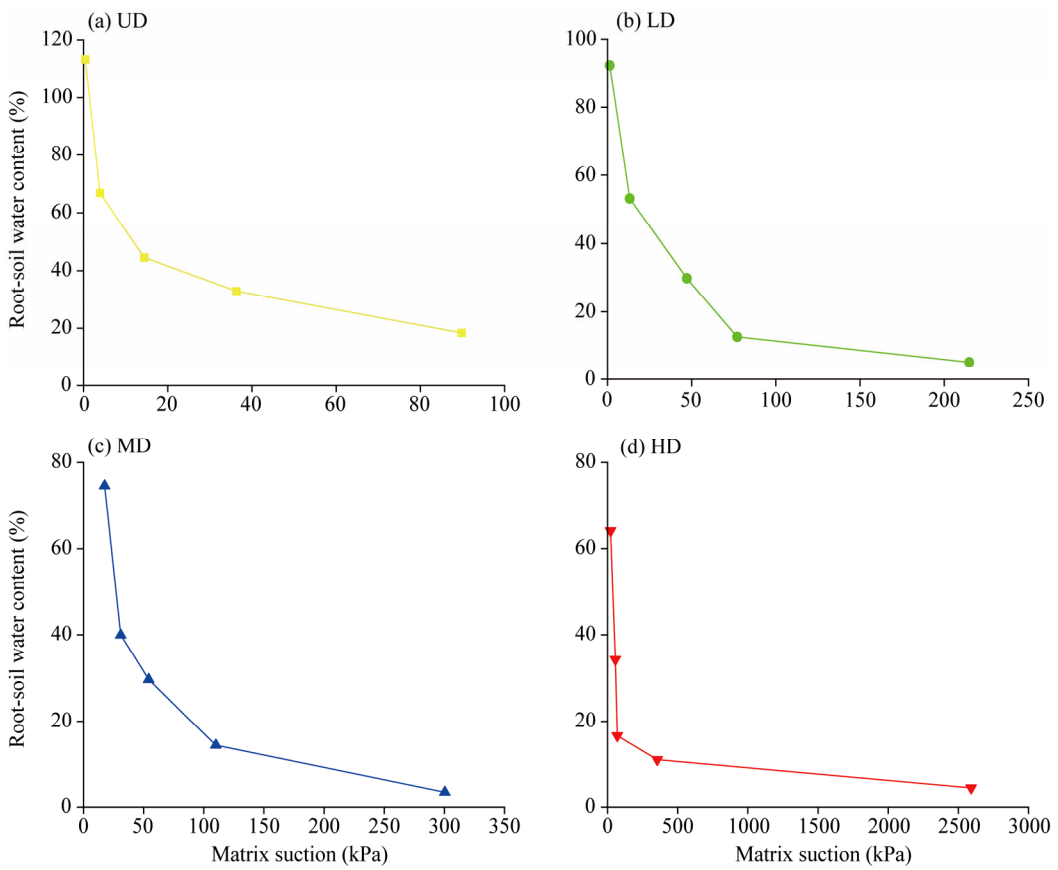

Fig. 8 Matrix suction characteristic curve of root-soil composite with different degrees of degradation. (a), UD; (b), LD; (c), MD; (d), HD.

coverage and the intertwining of roots, the root-soil water content was effectively maintained. As a result, the matrix suction only increased slightly as root-soil water content decreased from 113.34% to 12.59%. However, as the degree of degradation increased to LD to MD to HD, surface cracks formed and developed continuously. These cracks formed preferential flow pathways, leading to a decrease in the root-soil water content and a significant increase in the matrix suction. In particular, for the root-soil composites from MD and HD plots, the matrix suction increased dramatically, from 17.60 and 21.70 kPa to 300.40 and 2591.20 kPa, respectively, i.e., increases of 173.10% and 762.65%, respectively. Furthermore, due to differences in the water-holding capacity, root-soil mass ratio, and root-area ratio of root-soil composites with different degrees of degradation, the root-soil water content at which the matrix suction reached the minimum value also varied, with UD at 113.34%, LD at 92.44%, MD at 75.47%, and HD at 64.07%.

The degradation process of alpine meadow alters soil structure, leading to reduction in the root-soil water content, which in turn affects the rate of change in matrix suction. As shown in Figure 9, with increasing drying time, the rate of change in matrix suction increased firstly and then decreased. For the root-soil composites from UD and LD plots, the strong water-holding capacity and relatively simple evolution of surface cracks resulted in slow water evaporation, leading to a gentler rate of change in matrix suction. As the degradation intensified, the cracks expanded and began to connect, accelerating water evaporation and increasing the rate of change in matrix suction. For the root-soil composite from the MD plot, the rate of change in matrix suction increased to 10.46 kPa/h during the drying time period of 96–108 h. For the root-soil composite from the HD plot, the cracks evolved into a composite polygonal network structure, which significantly increased the water loss from the root-soil composite. As a result, during the drying time of 84–96 h, the rate of change in matrix suction of the root-soil composite from the HD plot sharply increased to 122.98 kPa/h.

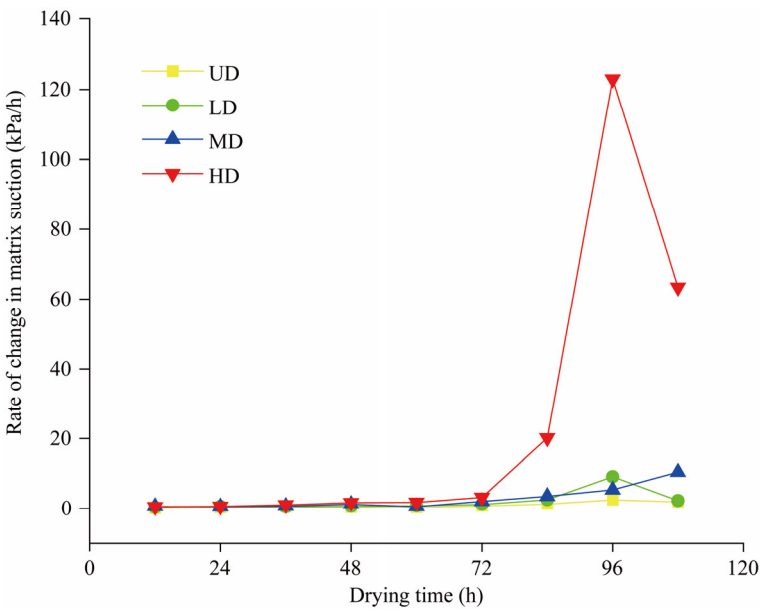

Fig. 9 Rate of change in matrix suction of root-soil composites with different degrees of degradation

4.4 Relationship among root-soil water content, matrix suction, and tensile strength

In the three-dimensional fitted surface, tensile strength was used as the independent variable and matrix suction and root-soil water content as dependent variables. Matlab software was used to derive the linear fitting equations for root-soil water content, tensile strength and

matrix suction:

$$P' = 50.823 - 22.06w_{sr} - 0.0008874\varphi, \quad (11)$$

where P' is the model-predicted tensile strength of root-soil composite (kPa); and φ is the matrix suction of root-soil composite (kPa). The fitting equation yielded an R^2 value of 0.726, indicating that the tensile strength of root-soil composite was negatively correlated with the root-soil water content and matrix suction.

According to Figure 10a, the tensile strength and matrix suction of the root-soil composites increased with decreasing root-soil water content in the three-dimensional fitted surface. At the curved plane, increased matrix suction significantly slowed root-soil water content reduction. Along the y-axis, the surface-generated matrix suction shifted slightly toward higher matrix suction as the tensile strength of root-soil composite increased. This demonstrated the model can predict the effects of root-soil water content and matrix suction on the tensile strength of the root-soil composites.

To further analyse the factors influencing the soil-water characteristics of the root-soil composites with different degrees of degradation, combined with the fitting results of the soil-water characteristic surface of root-soil composite, the fitting values and experimental values were substituted into the fitting formula, and the fitting relationship between the matrix suction and tensile strength of the root-soil composites from the study area was obtained (Fig. 10b). When the matrix suction force exceeded 100.00 kPa, the calculated tensile strength values closely resembled the experimental values, with a relative error range of 1.91%–15.73%. When the matrix suction force was less than 100.00 kPa, the calculated values exhibited a significant deviation from the experimental values, with an error exceeding 20.00%. This discrepancy primarily arises from the assumption in the theoretical model that the indoor conditions are relatively stable. The actual alpine meadow root-soil composites are affected by many factors. The failure to fully simulate the changes in the natural state resulted in a significant deviation in the results.

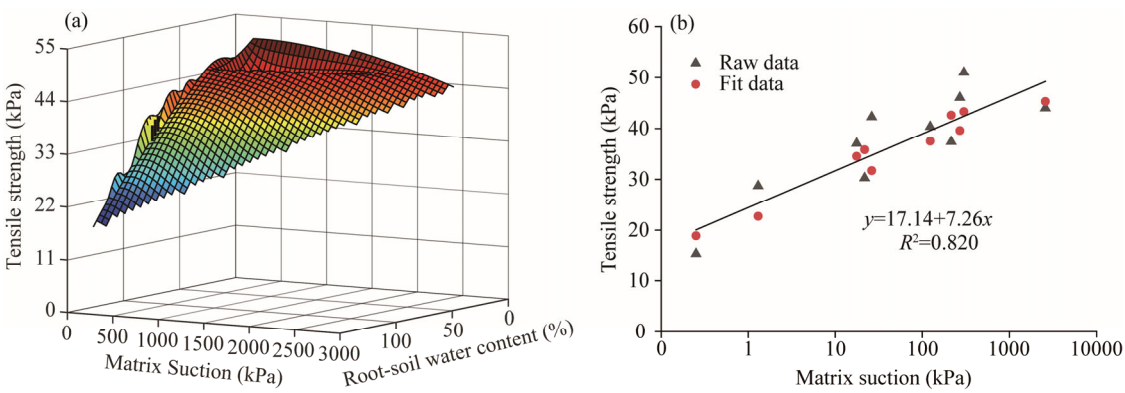

Fig. 10 Relationship among root-soil water content, matrix suction and tensile strength. (a), fitting surface diagram; (b), simulation formula between tensile strength and matrix suction.

4.5 Relationship between surface crack and soil properties

When the root-soil water content decreased to 30.00%–40.00%, the tensile stress in the surface layer of the alpine meadows exceeded both the interconnection strength between soil particles and the tensile resistance of plant roots, leading to the formation of micro-cracks in the surface layers of the LD, MD, and HD plots. At this point, the matrix suction values of the root-soil composites from the LD, MD, and HD plots ranged from approximately 50.00 to 100.00 kPa, surpassing their tensile strengths (Fig. 11a). The relationship among the root-soil mass ratio, matrix suction, and tensile strength in alpine meadow plots with different degrees of degradation (Fig. 11b) showed that as the meadow degradation intensified, the thickness

of felt layer increased from 3.00–4.00 cm in the root-soil composite of the UD plot to 7.00 cm in the root-soil composite of the MD plot. Simultaneously, the root-soil mass ratio increased from 13.58% to 22.29%, increasing the density of root-soil composite and reducing its water-holding capacity. As a result, the tensile strength and matrix suction of root-soil composite from the MD plot increased by 27.24 kPa and 47.10 kPa, respectively, compared with the root-soil composite from the UD plot. However, in the root-soil composite from the HD plot, although the felt layer continued to thicken, the root-soil mass ratio declined significantly as the dominant plant species became progressively more weed-dominated, which lowered the tensile strength to 41.36 kPa. In addition, as the cracks in the root-soil composite from the HD plot evolved into a complex polygonal network, the distribution of mouse holes, bare land, and collapsed areas increased, accelerating water loss and leading to a corresponding increase in the matrix suction.

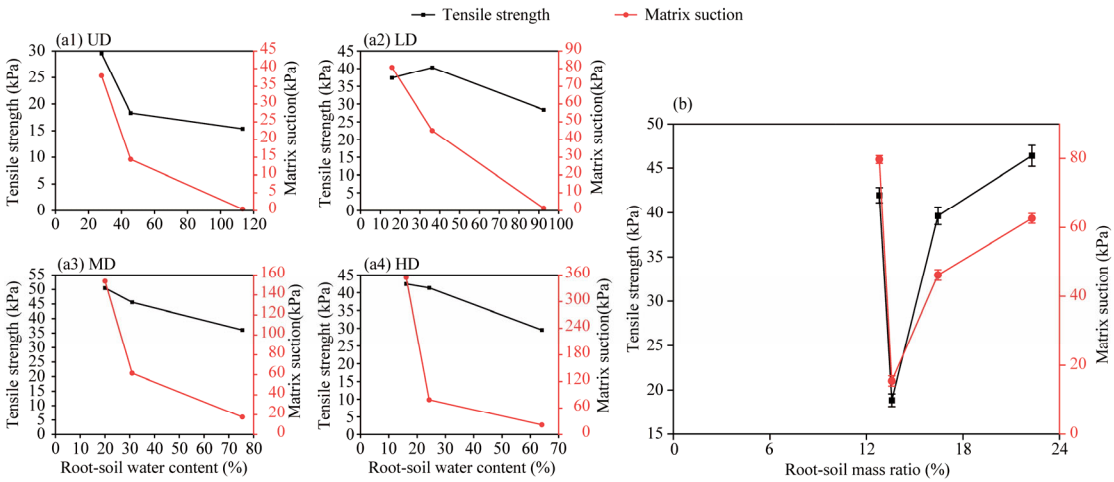

Fig. 11 Variation trend in matrix suction and tensile strength of root-soil composites from different degrees of degradation with water content (a) and root content (b) changes.

5 Discussion

5.1 Effects of the degradation of alpine meadows on the mechanics of root-soil composite

As the degradation of alpine meadows intensifies, meadow productivity progressively declines. The vegetation community alters significantly in coverage, aboveground biomass, and belowground biomass, with concomitant changes in root distribution and growth patterns within soil (Wen et al., 2013). During the degradation process from UD to MD, plant roots adapt to environmental changes by developing dwarfed aboveground vegetation while dramatically increasing root-soil mass ratio in shallow soil layers. The maximum increases in root-soil mass ratio and root area ratio reached 64.14% and 119.05%, respectively. This was consistent with the conclusion of Wu et al. (2024) that the root system degenerates in alpine meadows and root-soil mass ratio increases, while a large number of root systems are intertwined during the degradation process, gradually forming a dense and stable grass felt layer. However, with the intensification of degradation, the structure of vegetation communities varied in alpine meadows, and dominant species gradually evolved from grass family and sedge family plants with developed root systems to mixed grass vegetation with weaker mechanical strength and fewer numbers (Wen et al., 2013), resulting in a decrease in the root-soil mass ratio and root area ratio during the HD stage, which was 1.74 and 1.86 times respectively compared with the MD stage. The mechanical support and reinforcement

provided by the root system of root-soil composite weakens, the structure becomes loose, and the mechanical characteristics of root-soil composite also reduce (Zhang et al., 2024).

Meadow degradation makes soil tighter. The dry density of root-soil composites increased by 69.20% from UD to HD stage. The increase in soil compactness reduces water infiltration and easily forms runoff on the land surface, as well as takes away nutrients and fine grain from soil. The content of fine grain (<0.075 mm) dropped from 25.70% in the UD plot to 8.70% in the HD plot, and the soil structure was reorganized (Niu et al., 2021), thereby weakening the mechanical strength of root-soil composite. The continuous reduction of infiltration capacity makes it difficult to replenish water to soil in time, affecting the water absorption and storage function of root system, resulting in a decrease in the root-soil's ability to hold water (Sha et al., 2024), making the root-soil composite more prone to water loss under drought conditions, further becoming prone to dryness and cracking, and finally, the connection between the root system and the soil becoming unsolid (Zhang et al., 2024). In addition, due to excessive grazing and biological trampling and eating activities, such as plateau rats and rabbits, soil agglomerations in alpine meadows are increasingly broken, the root-soil composite structure damages and its resistance reduces. Besides, natural forces, such as wind erosion and water erosion, are more likely to migrate soil particles and tend to coarse.

To sum up, the degradation of alpine meadow causes complex changes in plant composition, root system characteristics, and soil structure, which also changes the mechanical strength of root-soil composite accordingly, and the soil strength and structural integrity are also damaged.

5.2 Mechanics of surface cracking of alpine meadow

Soil drying is a complex multi-physics coupling process that involves water evaporation, volume shrinkage, and soil cracking (Qing et al., 2023). As water evaporated from soil, the soil water state transforms from saturated to unsaturated. The reduction in water content increases the matrix suction and causes soil shrinkage, which in turn generates a tensile stress field within the soil. When the magnitude of tensile stress exceeds the soil's tensile strength, cracks begin to form (Tang et al., 2010; Tang et al., 2021). In the initial stage of constant water evaporation, the root-soil composite samples from alpine meadow with different degrees of degradation refilled with water in the pores of plant roots and soil particles. At this point, the soil matrix suction for the root-soil composites from the UD, LD, MD, and HD plots were the lowest, with values of 0.40, 1.30, 17.60, and 21.70 kPa, respectively. As the drying time increased, the free water between soil particles evaporated, aided by plant transpiration. This led to the capillary effect, through which the spacing between the soil particles and the size of pores become smaller, resulting in an increase in the matrix suction (Ni et al., 2017; Tang et al., 2018). The matrix suction of the root-soil composites from the LD, MD, and HD plots exceeded 50.00 kPa, when root-soil water content was less than 30.00%. Based on this and the crack development process observed during the drying test (Fig. 12), the critical root-soil water content range corresponding to the first appearance of micro-cracks in the surfaces of the LD, MD, and HD large ring cutter samples was 30.00%–40.00%. The value of root-soil water content at the point of micro-crack appearance is slightly higher than the critical water content of soil for desiccation cracking in cohesive soil slurry (Gu et al., 2023). This discrepancy primarily arises from the differences in the micro-structures of root-soil composites and the slurry samples, as well as the water-retention capacity of vegetation in samples (Gu et al., 2023). As root-soil water content decreased and entered the deceleration phase, the amount of free water between soil particles gradually decreases, and soil particle spacing and pore size are getting smaller. The matrix suction of the root-soil composites from the LD, MD, and HD plots exceeded 100.00 kPa, surpassing their tensile strengths, which is consistent with the findings of Yesiller et al. (2000) and Peron et al. (2009b). As evaporation continues, capillarity causes the pore radius of soil particles to decrease and soil particles to become more compact, which provides an incentive for cracks to deepen and expand (Al-

Mayahi et al., 2023). Eventually, cracks in root-soil composites of the LD, MD, and HD plots evolved into dendritic and polygonal shapes.

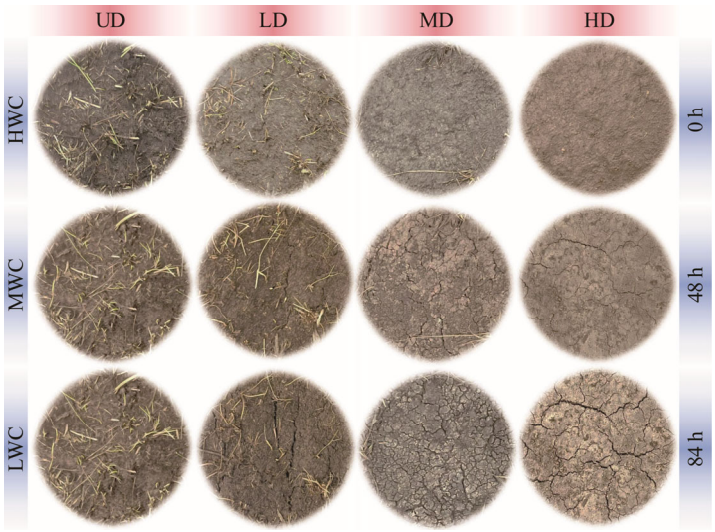

Fig. 12 Images of crack development in root-soil composites during drying process

Matrix suction is approximately linearly correlated with decreasing evapotranspiration rates (Wilson et al., 1997). In alpine meadow ecosystems on the Xizang Plateau, the root-soil water content, root-soil composite pore space, and plant root system all directly influence the changes in root-soil matrix suction (Li et al., 2013; Ni et al., 2017). When the root-soil water content continually decreasing, the contact between root and soil particle becomes more thorough, the soil structure reaches its shrinkage limit, and the crack width stabilizes (Tang et al., 2018).

To sum up, when the root-soil water content decreased from 113.34% to 0.00%, the matrix suction of root-soil composites in alpine meadows with different degradation degrees increased from 0.40 to 2591.20 kPa, which was significantly greater than the tensile strength of root-soil composite (15.38 to 50.49 kPa). Especially during the process of changing moisture conditions, the mechanical effect of matrix suction is significantly stronger in the regulation of soil cracking than tensile strength. It could be seen that among the two main influencing factors that controll the development of surface fractures in alpine meadows, matrix suction occupies an important position and is one of the key factors that dominate the development of fractures.

5.3 Limitations and prospects

In this study, we utilized root-soil composites from alpine meadow plots with different degrees of degradation to investigate the characteristics of surface crack development. Specially, we researched the contributions of soil mechanical parameter (tensile strength) and hydraulic parameter (matrix suction) to crack development. The influences of the changes in the root-soil water content on the tensile strength and matrix suction of root-soil composites were determined, and the mechanism of surface cracking in alpine meadows was also briefly analysed.

In the indoor simulation experiments, the constant temperature drying process used in this study cannot simulate the dynamic influence of the day-night temperature difference and wind speed on the evaporation rate of plateau on the changes in root-soil water content, which may lead to deviations in the critical water content threshold of root-soil composite cracking. In addition, the freeze-thaw cycle in the plateau area has an important impact on the formation and development of soil cracks. The synergistic effect of freeze-thaw and dry-wet cycles has

a damaging effect on soil, which promotes changes in moisture in soil and deteriorates soil structure (Zhao et al., 2021), making the connection between soil particles lose, thereby increasing the generation and expansion of cracks. This is also an important factor in the development of soil cracks under natural conditions, and indoor simulation experiments have not yet considered this point. Subsequent studies should conduct *in situ* field monitoring to verify the universality of root-soil water content threshold. Additionally, it is essential to conduct in-depth research on the changes in the root composition, mechanical properties of root, and activity of alpine meadow vegetation, as well as the variations in soil particle composition and microstructure caused by alpine meadow degradation. The individual and synergistic effects of these factors on matrix suction and tensile strength of alpine meadow soil should be examined. It is imperative to conduct an in-depth analysis of surface crack initiation and evolution mechanisms in alpine meadows under the coupled effects of dry-wet and freeze-thaw cycles.

6 Conclusions

To elucidate the effects of alpine meadow degradation and root-soil water content changes on both the physical properties of root-soil composites and two key mechanical parameters governing surface crack development (matrix suction and tensile strength), this study directly conducted tensile and matrix suction tests. The results revealed that with progressive intensification of alpine meadow degradation, the dry density of root-soil composite exhibited an increasing trend, and the root-soil water content gradually decreased. Simultaneously, the soil particle composition exhibited a coarsening tendency, accompanied by an increase in the uniformity coefficient of particle size. Both the root-soil mass ratio and root area ratio initially increased and then decreased. By comparing the surface fissure development characteristics of each sample under different drying durations, it was found that the matrix suction and tensile strength of root-soil composite exhibited a tendency of decreasing and then increasing with the root-soil mass ratio. Comparing to other degradation degrees, the tensile strength of the root-soil composite from the MD plot at the three different water content gradients (LWC, MWC, and HWC) was the highest. In addition, both the tensile strength and matrix suction of root-soil composite tended to increase as the root-soil water content decreased. Comparative analysis of surface crack development during root-soil composite desiccation revealed that the critical water threshold for surface cracking in lightly, moderately, and severely degraded soils was 30.00%–40.00%. At the same time, the matrix suction of root-soil composite increased to 50.00–100.00 kPa, exceeding the tensile strength of root-soil composite at equivalent moisture degrees by approximately 1–2 times. In future studies, it is necessary to establish numerical simulations of the relationship between the development of surface soil cracks and root types, as well as their hydro-mechanical properties.

Conflict of interest

The authors declare that they have no known competing financial interests or personal relationships that could have appeared to influence the work reported in this paper.

Acknowledgements

This study was funded by the National Natural Science Foundation of China (42062019, 42002283). We thank all of the anonymous reviewers and editors for providing helpful comments on this manuscript.

Author contributions

Conceptualisation: ZHANG Hailong, ZHU Haili; Methodology: ZHANG Hailong, WU Yuechen, ZHU Haili; Field test guidance: LIU Yabin, LI Guorong; Indoor test guidance: HU Xiasong; Indoor and outdoor tests: ZHANG Hailong, WU Yuechen, XU Pengkai, HONG Chenze; Data curation: ZHANG Hailong, WU

Yuechen; Writing - original draft preparation: ZHANG Hailong; Writing - review and editing: ZHU Haili. All authors approved the manuscript.

References

Al-Mayahi A K, Al-Ismaily S S, Breitenstein D, et al. 2023. Soil water distribution and dynamics across prescribed capillary barriers under evaporating surfaces. Biosystems Engineering, 226: 55–70.

Cheng Q, Gu Y D, Tang C S, et al. 2024. Desiccation cracking behaviour of a vegetated soil incorporating planting density. Canadian Geotechnical Journal, 61(1): 165–173.

Cui L X, Cheng Q, So P S, et al. 2024. Relationship between root characteristics and saturated hydraulic conductivity in a grassed clayey soil. Journal of Hydrology, 645: 132231, doi: 10.1016/j.jhydrol.2024.132231.

Duan P, Zhang Y C, Wang J G, et al. 2020. Functional diversity of soil microbial communities during degradation of alpine wetlands in Qinghai-Tibet Plateau. Acta Agrestia Sinica, 28(3): 759–767. (in Chinese)

Fan B, Lin L, Cao G M, et al. 2020. Relationship between plant roots and physical soil properties in alpine meadows at different degradation stages. Acta Ecologica Sinica, 40(7): 2300–2309. (in Chinese)

General Administration of Quality Supervision, Inspection and Quarantine of the People's Republic of China. 2004. Parameters for Degradation, Sandification, and Salification of Rangelands (GB19377-2003). [2024-12-01]. https://std.samr.gov.cn. (in Chinese)

Gholami M, Sadeghi H, Alipanahi P. 2024. Anisotropic hydraulic conductivity of as-compacted, bare and vegetated soils. Géotechnique, 74(1): 1–14.

Greve A, Andersen M S, Acworth R I. 2010. Investigations of soil cracking and preferential flow in a weighing lysimeter filled with cracking clay soil. Journal of Hydrology, 393(1–2): 105–113.

Gu Y D, Cheng Q, Tang C S, et al. 2023. Desiccation cracking behavior of vegetated soil with various dry densities. Chinese Journal of Geotechnical Engineering, 45(11): 2420–2428. (in Chinese)

He D Q, Lu H J, Hu X S, et al. 2025. Mechanical properties and enhanced soil shear strength of herbaceous plant roots in the alpine meadow layer of the permafrost region on the Qinghai-Xizang Plateau, China. Journal of Arid Land, 17(4): 515–537.

Huang W, Xiang W, Wang J E, et al. 2018. Development and application of digital image processing technology based soil tensile apparatus. Rock and Soil Mechanics, 39(9): 3486–3494. (in Chinese)

Immerzeel W W, Van Beek L P H, Bierkens M F P. 2010. Climate change will affect the Asian water towers. Science, 328(5984): 1382–1385.

Leung K A, Garg A, Ng W W C. 2015. Effects of plant roots on soil-water retention and induced suction in vegetated soil. Engineering Geology, 193: 183–197.

Li B F, Zhu H L, Xie B S, et al. 2020. Study on tensile properties of root-soil composite of alpine meadow plants in the riparian zone of the Yellow River source region. Chinese Journal of Rock Mechanics and Engineering, 39(2): 424–432. (in Chinese)

Li T, Liu B, Yang W H, et al. 2013. Experimental research on the influence of matrix suction on the shear strength of remolded red clay. Journal of China University of Mining and Technology, 42(3): 375–381. (in Chinese)

Liu Q, Su L J, Xia Z Y, et al. 2019. Effects of soil properties and illumination intensities on matric suction of vegetated soil. Sustainability, 11(22): 6475, doi: 10.3390/su11226475.

Lozada C, Caicedo B, Thorel L. 2015. Effects of cracks and desiccation on the bearing capacity of soil deposits. Géotechnique Letters, 5(3): 112–117.

Lu J R, Zhang Q, Werner A D, et al. 2020. Root-induced changes of soil hydraulic properties-A review. Journal of Hydrology, 589: 125203, doi: 10.1016/j.jhydrol.2020.125203.

Miehe G, Schleuss P M, Seeber E, et al. 2019. The *Kobresia pygmaea* ecosystem of the Tibetan highlands—Origin, functioning and degradation of the world's largest pastoral alpine ecosystem: *Kobresia pastures* of Tibet. Science of the Total Environment, 648: 754–771.

Ministry of Housing and Urban-Rural Development of the People's Republic of China. Standard for Geotechnical Testing Method (GB/T50123-2019). [2024-12-10]. https://www.mohurd.gov.cn. (in Chinese)

Ni J J, Leung A K, Ng C W W, et al. 2017. Investigation of plant growth and transpiration-induced matric suction under mixed grass-tree conditions. Canadian Geotechnical Journal, 54(4): 561–573.

Niu Y J, Yang S W, Zhu H M, et al. 2021. Plant community distribution induced by microtopography due to soil cracks developed in overgrazed alpine meadows on the Tibetan Plateau. Land Degradation & Development, 32(11): 3167–3179.

Peron H, Hueckel T, Laloui L, et al. 2009a. Fundamentals of desiccation cracking of fine-grained soils: experimental characterisation and mechanisms identification. Canadian Geotechnical Journal, 46(10): 1177–1201.

Peron H, Laloui L, Hueckel T, et al. 2009b. Desiccation cracking of soils. European Journal of Environmental and Civil Engineering, 13(7–8): 869–888.

Preti F, Giadrossich F. 2009. Root reinforcement and slope bioengineering stabilization by Spanish Broom (*Spartium junceum* L). Hydrology and Earth System Sciences, 13(9): 1713–1726.

Qing Y M, Wang S, Yang Z L, et al. 2023. Accelerated soil drying linked to increasing evaporative demand in wet regions. npj Climate and Atmospheric Science, 6(1): 205, doi: 10.1038/s41612-023-00531-y.

Schwarz M, Cohen D, Or D. 2010. Root‐soil mechanical interactions during pullout and failure of root bundles. Journal of Geophysical Research: Earth Surface, 115(F4): 1–19.

Sha S L, Cai G C, Liu S R, et al. 2024. Roots to the rescue: how plants harness hydraulic redistribution to survive drought across contrasting soil textures. Advanced Biotechnology, 2(4): 43, doi: 10.1007/s44307-024-00050-8.

Tang C S, Cui Y J, Tang A M, et al. 2010. Experiment evidence on the temperature dependence of desiccation cracking behavior of clayey soils. Engineering Geology, 114(3–4): 261–266.

Tang C S, Cui Y J, Anh-minh T, et al. 2012. Shrinkage and desiccation cracking process of expansive soil and its temperature-dependent behaviour. Chinese Journal of Geotechnical Engineering, 34(12): 2181–2187. (in Chinese)

Tang C S, Shi B, Cui Y J. 2018. Behaviors and mechanisms of desiccation cracking of soils. Chinese Journal of Geotechnical Engineering, 40(8): 1415–1423. (in Chinese)

Tang C S, Zhu C, Cheng Q, et al. 2021. Desiccation cracking of soils: A review of investigation approaches, underlying mechanisms, and influencing factors. Earth-Science Reviews, 216: 103586, doi: 10.1016/j.earscirev.2021.103586.

Victor S, Hua L M. 2010. North-west China's rangelands and peoples: facts, figures, challenges and responses. Towards Sustainable Use of Rangelands in North-West China. Dordrecht: Springer, 3–18.

Wang Y F, Fan J, Jia M L. 2016. Variation of soil water content during vegetation restoration in the water-wind erosion crisscross region on the Loess Plateau. Acta Agrestia Sinica, 24(2): 344–350. (in Chinese)

Wen L, Dong S K, Li Y Y, et al. 2013. The impact of land degradation on the C pools in alpine grasslands of the Qinghai-Tibet Plateau. Plant and Soil, 368(1): 329–340.

Wilson G W, Fredlund D G, Barbour S L. 1997. The effect of soil suction on evaporative fluxes from soil surfaces. Canadian Geotechnical Journal, 34(1): 145–155.

Wu Y C, Zhu H L, Zhang Y, et al. 2024. Characterization of alpine meadow surface crack and its correlation with root-soil properties. Journal of Arid Land, 16(6): 834–851.

Xiong D H, Lu X N, Xian J S, et al. 2008. Selection of judging indicators for surface morphology of soil crack under different development degrees in Yuanmou Arid-hot Valley Region. Wuhan University Journal of Natural Sciences, 13(3): 363–368.

Xu Q L, Tang C S, Liu C L, et al. 2018. Review on soil desiccation cracking behavior and the mechanism related to fracture mechanics. Journal of Earch Sciences and Environment, 40(2): 223–236. (in Chinese)

Yesiller N, Miller C J, Inci G, et al. 2000. Desiccation and cracking behavior of three compacted landfill liner soils. Engineering Geology, 57(1–2): 105–121.

Yildiz A, Graf F, Rickli C, et al. 2019. Assessment of plant-induced suction and its effects on the shear strength of rooted soils. Proceedings of the Institution of Civil Engineers-Geotechnical Engineering, 172(6): 507–519.

Yuliana Y, Apriyono A, Kamchoom V, et al. 2025. Seasonal dynamics of root growth and desiccation cracks and their effects on soil hydraulic conductivity. Engineering Geology, 349: 107973, doi: 10.1016/j.enggeo.2025.107973.

Zhang H L, Zhu H L, Zhang Y, et al. 2024. Tensile and shear characteristics and influencing factors of root-bearing soil in alpine meadow on bank of Yellow River Source. Bulletin of Soil and Water Conservation, 44(5): 58–57. (in Chinese)

Zhang Z B, Zhou H, Zhao Q G, et al. 2014. Characteristics of cracks in two paddy soils and their impacts on preferential flow. Geoderma, 228–229: 114–121.

Zhao G T, Han Z, Zou W L, et al. 2021. Influences of drying-wetting-freeze-thaw cycles on soil-water and shrinkage characteristics of expansive soil. Chinese Journal of Geotechnical Engineering, 43(6): 1139–1146.

Zheng S H. 2003. Cracking behavior of expansive soil and slope stability analysis subject to rainfall infiltration. MSc Thesis. Shanghai: Shanghai Jiao Tong University. (in Chinese)

Zhou Y Y, Wang X M. 2019. Mesomechanics characteristics of soil reinforcement by plant roots. Bulletin of Engineering Geology and the Environment, 78: 3719–3728.